

**Guilhem Michon**

ISAE-DMSM,  
10 Avenue Edouard Belin,  
31055 Toulouse, France  
e-mail: guilhem.michon@supaero.fr

**Lionel Manin**

LaMCoS,  
INSA-Lyon, CNRS 5259,  
F69621, France  
e-mail: lionel.manin@insa-lyon.fr

**Robert G. Parker**

Department of Mechanical Engineering,  
The Ohio State University,  
650 Ackerman Road,  
Columbus, OH 43202  
e-mail: parker.242@osu.edu

**Régis Dufour**

LaMCoS,  
INSA-Lyon, CNRS 5259,  
F69621, France  
e-mail: regis.dufour@insa-lyon.fr

# Duffing Oscillator With Parametric Excitation: Analytical and Experimental Investigation on a Belt-Pulley System

*This paper is devoted to the theoretical and experimental investigation of a sample automotive belt-pulley system subjected to tension fluctuations. The equation of motion for transverse vibrations leads to a Duffing oscillator parametrically excited. The analysis is performed via the multiple scales approach for predicting the nonlinear response, considering longitudinal viscous damping. An experimental setup gives rise to nonlinear parametric instabilities and also exhibits more complex phenomena. The experimental investigation validates the assumptions made and the proposed model.*

[DOI: 10.1115/1.2908160]

*Keywords:* Duffing oscillator, parametric instabilities, multiple scales, automotive belt, experimental investigation

## 1 Introduction

Multiribbed belts are commonly used to drive the automotive engine accessories (water pump, aircooling compressor, aided steering pump, etc.). These belts run over the accessory pulleys in a serpentine configuration so called the front end accessory drive (FEAD) [1,2]. The advantages of serpentine drives over classical V-belts include simplified assembly and replacement, longer belt life, tension compensation from tensioner device, and compactness. This system is subjected to numerous linear and nonlinear phenomena: belt-pulley slippage [3,4], time-varying boundary conditions of each belt span between two successive pulleys [5], hysteretic behavior due to mechanical [6,7] or hydraulic tensioners, and parametric excitations due to crankshaft torque pulsations that introduce a pulsating tension in the belt [8].

Moreover, in the instability zone, the belt exhibits large transverse deflection such as a Duffing oscillator with parametric excitation. For example, such nonlinear oscillations have been numerically and experimentally investigated by Pellicano et al. [9] by using a specific device comprising two pulleys, one of them imposing parametric excitation by the way of eccentric pulley mounting. See also the theoretical nonlinear dynamic analysis of an axially moving string parametrically excited of Mockenstrum et al. [10,11]. Similar behaviors are observed in cable [12–14], drill string [15], and rod parametrically excited by a force or a torque [16].

Reducing the impact of this large transverse deflection on the belt life requires to improve the knowledge on these nonlinear phenomena. This article deals with one of the modeling steps of the nonlinear global behavior of the entire FEAD. Its purpose is based on a theoretical and experimental investigation, limited to a nonmoving belt-pulley system parametrically excited, leading to lateral instabilities, Duffing oscillations (frequency response function with jump and hysteresis phenomena), and other observed nonlinear phenomena.

In the theoretical part, the equation including Duffing term and parametric excitation is established. By using the multiple scales method, the nonlinear response amplitude is predicted by keeping all of the nonlinear terms and the longitudinal viscous damping. The experimental part permits, apart from identifying the longitudinal and transverse belt moduli, measuring transverse vibrations on a sample belt-pulley setup equipped with automotive mechanical components. Finally, predicted and measured results are compared with regard to the nonlinear response and instability region determination.

## 2 Mechanical Model

**2.1 Equation of Motion.** A mechanical model of an axially moving beam subjected to tension fluctuation is used to predict the nonlinear response and the parametric instability region transition curves. The equation of motion for transverse vibration of a beam of length  $L$  moving with time dependent transport velocity  $c(T)$  is governed by [17]

$$\rho A (V_{,TT} + c_{,T} V_{,TX} + 2c V_{,TX} + c^2 V_{,XX}) - (P_s + P_d(T)) V_{,XX} + EI V_{,XXXX} = 0 \quad (1)$$

where  $\rho A$  is the mass per unit length,  $EI$  is the transverse rigidity modulus,  $V$  is the transverse displacement,  $P_s$  is the static belt tension,  $P_d(T)$  is the dynamic tension, and  $T$  and  $X$  are the temporal and spatial variables. The dynamic tension is due to longitudinal motion of the end points from pulley oscillations and quasi-static midplane stretching from transverse deflection, and is given by

$$P_d(T) = \frac{EA}{L} \left[ U(L, T) - U(0, T) + \frac{1}{2} \int_0^L V_{,X}^2 dX \right] + \eta A \int_0^L V_{,X} V_{,XT} dX \quad (2)$$

where  $EA$  is the longitudinal rigidity modulus,  $\eta$  is the longitudinal damping, and  $U$  is the longitudinal displacement. With the dimensionless parameters

Contributed by the Design Engineering Division of ASME for publication in the JOURNAL OF COMPUTATIONAL AND NONLINEAR DYNAMICS. Manuscript received September 15, 2006; final manuscript received September 10, 2007; published online April 30, 2008. Review conducted by Claude-Henri Lamarque.

$$x, v, u = \frac{X, V, U}{L}, \quad t = T \sqrt{\frac{P_s}{\rho A L^2}}, \quad \gamma = c \sqrt{\frac{\rho A}{P_s}}, \quad (3)$$

$$\xi = \eta \sqrt{\frac{A}{\rho P_s L^2}}, \quad \zeta = \frac{EA}{P_s}, \quad \mu = \frac{EI}{P_s L^2}, \quad \Omega_i = \sqrt{\frac{\rho A L^2}{P_s}} \bar{\Omega}_i$$

Eq. (1) becomes

$$v_{,tt} + 2\gamma v_{,tx} + \gamma_t v_{,x} - (1 - \gamma^2) v_{,xx} + \mu v_{,xxxx} - \zeta v_{,xx} \left[ u(1, t) - u(0, t) + \frac{1}{2} \int_0^1 v_{,x}^2 dx \right] - 2\xi v_{,xx} \int_0^1 v_{,x} v_{,xt} dx = 0 \quad (4)$$

In the case of a long, nonmoving ( $\gamma=0$ ) belt span preloaded with a high static tension and subjected to sinusoidal tension fluctuation, the transverse stiffness is dominated by tension ( $\mu$  is neglected, see Sec. 3.1). The tension fluctuation is given by

$$\zeta \left( u(1, t) - u(0, t) + \frac{1}{2} \int_0^1 v_{,x}^2 dx \right) + 2\xi \int_0^1 v_{,x} v_{,xt} dx = \varepsilon \left( \cos(\Omega t) + \int_0^1 \left( \frac{\alpha}{2} v_{,x}^2 + 2\chi v_{,x} v_{,xt} \right) dx \right) \quad (5)$$

where  $\varepsilon = P_d/P_s$  represents the ratio of the dynamic tension fluctuation to the static span tension,  $\alpha = \zeta/\varepsilon$  is the coefficient of the nonlinear term, and  $\chi = \xi/\varepsilon$  is related to the longitudinal damping. Then, Eq. (4) leads to

$$v_{,tt} - \left( 1 + \varepsilon \cos(\Omega t) + \varepsilon \int_0^1 \left( \frac{\alpha}{2} v_{,x}^2 + 2\chi v_{,x} v_{,xt} \right) dx \right) v_{,xx} = 0 \quad (6)$$

By considering the single mode Galerkin expansion  $v(x, t) = a_n(t) \psi_n(x)$  with the basis  $\psi_n(x) = \sin(n\pi x)/n\pi$ , Eq. (6) becomes a parametrically excited Duffing equation

$$\ddot{a}_n + (\omega_n^2 + n^2 \pi^2 \varepsilon \cos(\Omega t)) a_n + n^2 \pi^2 \frac{\varepsilon}{4} \alpha a_n^3 + n^2 \pi^2 \varepsilon \chi \dot{a}_n a_n^2 = 0 \quad (7)$$

where  $\omega_n = n\pi$  are the natural frequencies of a tensioned string.

The small transverse response of a simply supported belt span subjected to a harmonic tension is governed by a set of uncoupled Mathieu's equations and exhibits instability regions based on  $\Omega_k^n = 2\omega_n/k$ , where  $k$  is the instability order and  $\omega_n$  is the  $n$ th resonance pulsation. Modeling large transverse deflection brings a cubic term in the proposed equation. With the presence of this odd-order nonlinearity, the single mode expansion remains reasonable and is justified by the agreement with the experimental results of Sec. 4.

**2.2 Nonlinear Forced Response.** Experimental observations show that the lateral vibration amplitude is sufficiently large that the system equation cannot be linearized. To solve the response of the system for primary resonance ( $\Omega \approx 2\omega$ ) of the first mode ( $a_n = a$ ,  $\omega_n = \omega$ ), a first order multiple scales method is used [18]. The independent time variable is a function of multiple scales  $T_0 = t$  and  $T_1 = \varepsilon t$ . Then,

$$a(t, \varepsilon) = a_0(T_0, T_1) + \varepsilon a_1(T_0, T_1) \quad (8)$$

Substituting Eq. (8) into Eq. (7) and equating coefficients of like powers of  $\varepsilon$  yields

$$D_0^2 a_0 + \omega^2 a_0 = 0 \quad (9)$$

$$D_0^2 a_1 + \omega^2 a_1 = -2D_0 D_1 a_0 - \pi^2 \chi D_0 a_0 a_0^2 - \pi^2 \cos(\Omega T_0) a_0 - \frac{\pi^2}{4} \alpha a_0^3 \quad (10)$$

where  $D_0$  and  $D_1$  indicate differentiation with respect to  $T_0$  and  $T_1$ . The solution of Eq. (9) is

$$a_0 = A(T_1) e^{i\omega T_0} + \bar{A}(T_1) e^{-i\omega T_0} \quad (11)$$

Introducing the frequency expansion  $\Omega = 2\omega + \varepsilon\sigma$  and eliminating the secular terms in Eq. (10) lead to

$$-2i\omega D_1 A - i\pi^2 \chi \omega A^2 \bar{A} - \frac{\pi^2}{2} \bar{A} e^{i\sigma T_1} - \frac{3\pi^2}{4} \alpha A^2 \bar{A} = 0 \quad (12)$$

with the substitutions  $A = (\lambda/2) e^{i\beta}$ , with  $\lambda$  and  $\beta$  real, and  $\nu = \sigma T_1 - 2\beta$ ; the equations governing amplitude and phase are

$$\frac{d\lambda}{dT_1} = -\frac{1}{8} \pi^2 \chi \lambda^3 - \pi^2 \frac{\lambda}{4\omega} \sin(\nu) \quad (13)$$

$$\lambda \frac{d\nu}{dT_1} = \sigma \lambda - \frac{\pi^2 \lambda}{2\omega} \cos(\nu) - \frac{3}{16} \pi^2 \frac{\alpha}{\omega} \lambda^3 \quad (14)$$

From the equilibriums of Eqs. (13) and (14), nontrivial solutions for the steady state response are

$$\lambda = \frac{\sqrt{8(9\alpha^2 + 16\pi^2 \chi^2)(6\pi\sigma\alpha \pm \pi^2 \sqrt{9\alpha^2 + 16\pi^2 \chi^2 - 64\chi^2 \sigma^2})}}{\pi(9\alpha^2 + 16\pi^2 \chi^2)} \quad (15)$$

and

$$a(t) = \lambda \cos\left(\frac{\Omega}{2} t + \nu\right) + O(\varepsilon) \quad (16)$$

Recalling that  $\Omega = 2\omega + \varepsilon\sigma$  and introducing the new notation  $\hat{\sigma} = \varepsilon\sigma$ ,  $\hat{\alpha} = \alpha\varepsilon$ , and  $\hat{\chi} = \chi\varepsilon$  in order to exhibit  $\varepsilon$  influence, then  $\Omega = 2\omega + \hat{\sigma}$  and

$$\lambda = \frac{\sqrt{8(9\hat{\alpha}^2 + 16\pi^2 \hat{\chi}^2) \left( 6\pi \hat{\sigma} \hat{\alpha} \pm \pi^2 \varepsilon \sqrt{9\hat{\alpha}^2 + 16\pi^2 \hat{\chi}^2 - 64 \frac{\hat{\chi}^2 \hat{\sigma}^2}{\varepsilon^2}} \right)}}{\pi(9\hat{\alpha}^2 + 16\pi^2 \hat{\chi}^2)} \quad (17)$$

### 3 Experimental Investigation

An experimental investigation is conducted in order to observe the predicted phenomenon and to validate the mechanical model.

**3.1 Belt Characteristic Identification.** To establish the model parameters for practical serpentine drives, an automotive belt is experimentally examined to extract its longitudinal and lateral elastic moduli and viscous damping.

**3.1.1 Longitudinal Elastic Modulus.** Experimentally, the belt is stretched between two pulleys for several static tensions. Its longitudinal stretching is captured with two laser sensors directed at two targets perpendicular to the belt axis at a known separation distance. The longitudinal stretching of the span is assumed to be linearly related to the static tension  $P_s$  according to  $P_s = EA(\Delta L/L)$ . The longitudinal stiffness results from the linear fitting of the tension/stretching relation and leads to the value  $EA = 110,000$  N.

**3.1.2 Longitudinal Viscous Damping.** A belt sample is clamped at one end and has a mass  $M$  suspended at the other. This system is excited via a shock hammer. The free response is re-

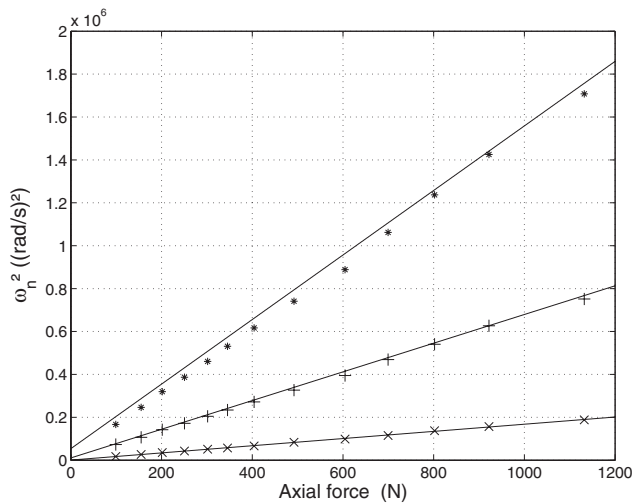


**Fig. 1 Square of the first three natural frequencies of a beam as a function of its tension, measured ( $\times$ ,  $+$ , and  $*$ ) and predicted (solid lines)**

corded via an accelerometer located under the mass and post-processed to obtain belt viscous damping and leads to the value of  $\eta=160$  N s/m.

**3.1.3 Lateral Elastic Modulus.** To estimate the bending stiffness, a transverse impact test is performed on a belt span for several initial tensions. The transverse vibration is captured with a laser sensor. The square of the  $n$ th transverse natural frequency  $\tilde{\omega}_n^2$  of a simply supported, stationary, tensioned beam is a linear function of the tension  $P_s$ ,

$$\tilde{\omega}_n^2 = EI \frac{n^4 \pi^4}{\rho A L^4} + P_s \frac{n^2 \pi^2}{\rho A L^2} \quad (18)$$

The evolution of the square of the first three natural frequencies versus  $P_s$  is presented in Fig. 1. When the tension  $P_s$  is nil, identification of  $EI$  for the first mode exhibits a small value of this modulus ( $EI=0.22$  N m<sup>2</sup> when  $\rho A=0.107$  kg/m and  $L=0.73$  m). This value introduced in Eq. (18) for the second and third modes shows only small difference with the experiment. By considering this small modulus and the span lengths of this application, the bending stiffness modulus is neglected. Thus, in the following, the belt span is considered as a string ( $\mu=0$ ).

**3.2 Experimental Setup of a Parametrically Excited Belt-Pulley System.** The setup is composed of an industrial, automotive, multiribbed belt tensioned in a three-pulley drive. A lever arm linked to one of the pulleys is connected to an electrodynamic shaker, as presented in Fig. 2. The tested belt span is  $L=0.46$  m, its cross section area is  $A=93.10^{-6}$  m<sup>2</sup>, its width being  $l=2.15$  cm, its mass density is  $\rho=1150$  kg/m<sup>3</sup>, and subjected to a static tension  $P_s=220$  N. It is composed of a ply of fiber cables having an angle with the longitudinal axis, molded within elastomer. The upper area is plane, while the lower one is composed of six ribs. The shaker applies an axial alternating force of amplitude  $f_1$  and frequency  $\eta$  to the lever arm, which creates tension fluctuation in the belt span. Thus, the system is parametrically excited. Instability will occur for lower frequencies in the upper span. The idler pulley in the lower span divides it into two shorter ones to avoid simultaneous instabilities in the lower and upper spans. The transmitted force is measured with a piezoelectric force sensor, and the transverse displacement of the upper span with a laser sensor.

This setup permits frequency sweeps (from 30 Hz to 150 Hz) with different amplitudes and static belt tensions. Figure 3 shows a visualization of the transverse vibration of the upper span under

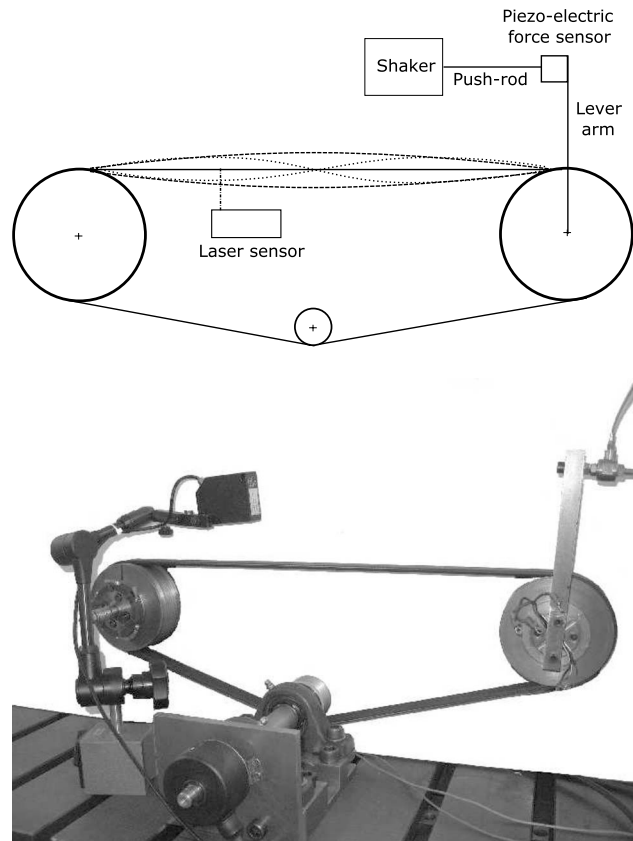


**Fig. 2 Parametric excitation experimental setup**

the primary instability region for  $\eta=2\tilde{\omega}_1$ . It exhibits the classical primary instability result: When the span is subjected to  $2\tilde{\omega}_1$ , its transverse vibration frequency is  $\tilde{\omega}_1$ . As an illustration, the peak-to-peak vibration amplitude is about 2 cm in the middle of the span.

**3.3 Observed Phenomena of a Parametrically Excited Belt-Pulley System.** The given model considers only a single belt span as a simply supported string. The experimental setup, however, consists of a circular belt wrapped around three pulleys, see also Fig. 2. Observations of other complex phenomena are obtained using a high speed camera capable of 1000 frames/s. For each following phenomenon, three different deformed positions are captured.

**3.3.1 Longitudinal and Transverse Coupling.** Consider the simplified model of the three pulley-shaft assembly rotational inertia linked by the belt longitudinal stiffness. This 3DOF model has a resonance at 80 Hz. The third lateral vibration mode of the upper span is close to 150 Hz, so the fourth instability region ( $\Omega=2\omega_3/4$ ) is in the vicinity of 75 Hz. Theoretically, observation of the instability region requires a large level of excitation that the available shaker is unable to produce. Due to the longitudinal resonance, the level of tension fluctuation increases and makes the parametric excitation of transverse instability based on higher natural frequencies possible. For instance, Fig. 4 shows such a phenomenon concerning the third mode shape of the tested belt span.

**3.3.2 Boundary Condition.** The multiribbed belt is wrapped around pulleys. While typically approximated as simply supported, the boundary condition is more complex, and uncertainty of the contact point condition makes definition of the boundary condition difficult. When it laterally vibrates, the length of the

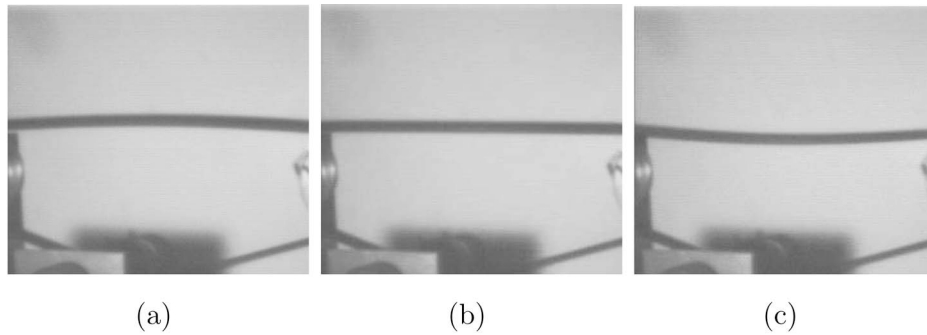


**Fig. 3 Three different positions captured with a high speed camera of the first mode shape of the tested belt span for the primary instability.  $\Omega=6.2$ ,  $\varepsilon=0.2$ .**

span is a function of time and varies approximately  $\pm 1$  cm as shown in Fig. 5 where the pulley diameter is 10 cm and the span length is 46 cm.

**3.3.3 Transverse-Torsional Coupling.** When the belt span is subjected to parametric tension fluctuations, large amplitudes of the first torsional mode are observed and captured, see Fig. 6. This is mostly due to the coupling between torsional and longitudinal modes initiated by the presence of the angle of fiber ply. Theoretical investigation of this coupling can be found in Refs. [19,20].

**3.3.4 Discussion on the Observed Phenomena.** The three previous phenomena are mainly due to either longitudinal-transverse or longitudinal-torsion couplings. They can be source of noise pollution, wear, efficiency loss, and belt failures in FEAD such as fatigue, leaving the pulley ribs and belt/pulley slippage.

## 4 Experimental Validation of the Proposed Model

The model developed in Sec. 2 permits comparing predicted and measured forced responses of the belt span.

**4.1 Instability Region.** The measured transverse instability regions of the belt span are gathered in the  $(\varepsilon, \Omega)$  diagram plotted in Fig. 7. The plotted dots stand for the observed transverse instability existence; they are provided by a step-by-step sweep up or down investigation for several levels of excitation amplitude  $\varepsilon$ . The constant space between points corresponds to the experimental forcing frequency step. In the primary region ( $\Omega \approx 2\omega$ ), the sweep up or down does not lead to the same left boundary: This is due to the hardening effect brought by the large transverse vibrations. To sum up, instability regions are wider when produced by a sweep up than those obtained by a sweep down forcing

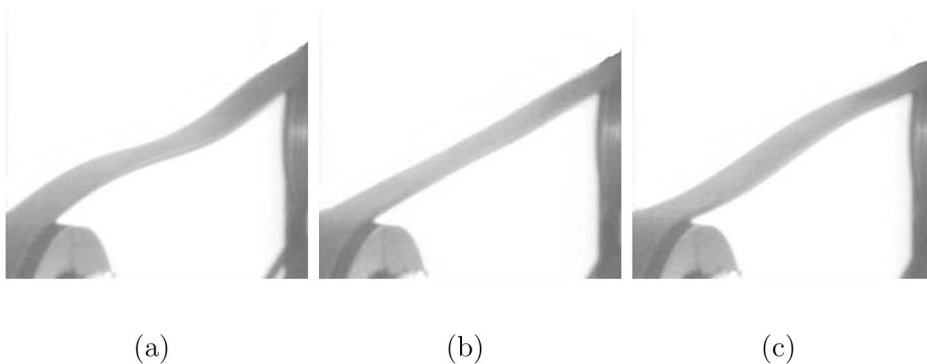


**Fig. 4 Three different positions captured with a high speed camera of the third mode shape of the tested belt span due to longitudinal-transverse coupling.  $\Omega=4.8$ ,  $\varepsilon=0.2$ .**

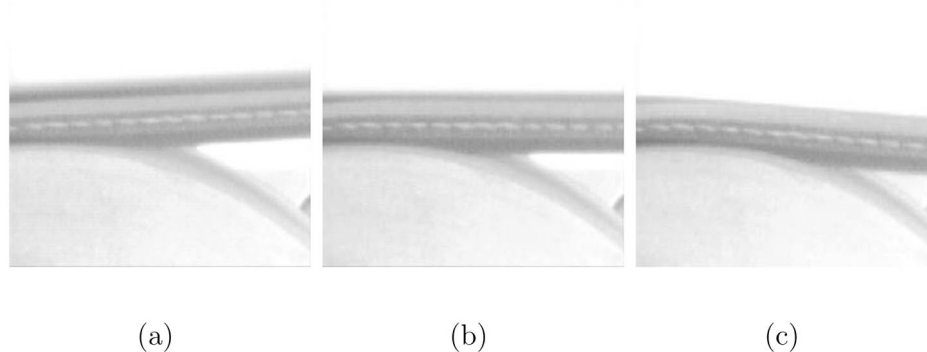


**Fig. 5 Three different positions captured with a high speed camera of a belt end showing the boundary condition evolution.  $\Omega=6.0$ ,  $\varepsilon=0.3$ .**

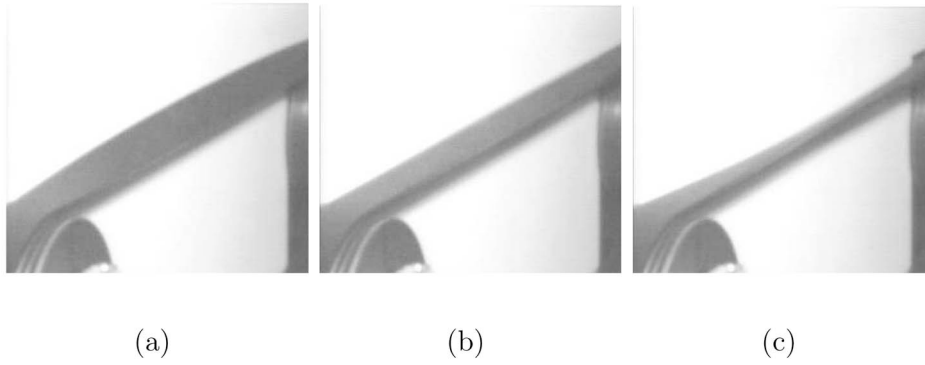


**Fig. 6** Three different positions captured with a high speed camera of torsion mode of the tested belt span due to longitudinal-torsion coupling.  $\Omega=5.6$ ,  $\varepsilon=0.12$ .

frequency.

In the secondary region ( $\Omega \approx \omega$ ), there is no hardening effect due to the small transverse vibration amplitudes.

**4.2 Frequency Response.** For a given forcing amplitude  $\varepsilon$ , the response amplitude  $\lambda$  in Eq. (17) is plotted versus the forcing frequency  $\Omega$  in Fig. 8. Nonreversible behavior and jump phenomena occur for changing excitation frequency. The swept-up sine investigation leads to a parametric instability phenomenon starting from  $\Omega=6$  to a jump down at  $\Omega=6.65$ . For a swept-down sine investigation, the resonance phenomenon starts by a jump up at  $\Omega=6.55$  and finishes at  $\Omega=6$ . The predicted response is very accurate concerning the beginning of the resonance phenomena and the jump up frequency. Nevertheless, the prediction of the jump down is overestimated by the model. This figure also compares the response with and without considering longitudinal damping of the belt. The presence of damping permits capturing the theoretical jump down frequency.

**4.3 Amplitude Response.** For a given forcing frequency  $\Omega$ , the response amplitude  $\lambda$  in Eq. (17) is plotted versus the forcing amplitude  $\varepsilon$  in Fig. 9. Sweeping  $\varepsilon$  highlights another type of hysteresis phenomenon. Predicted and measured responses are very close on the upper branch, but the jump location predictions are underestimated. This figure also compares the response with and without considering longitudinal damping of the belt. The presence of damping permits capturing the theoretical jump down frequency.

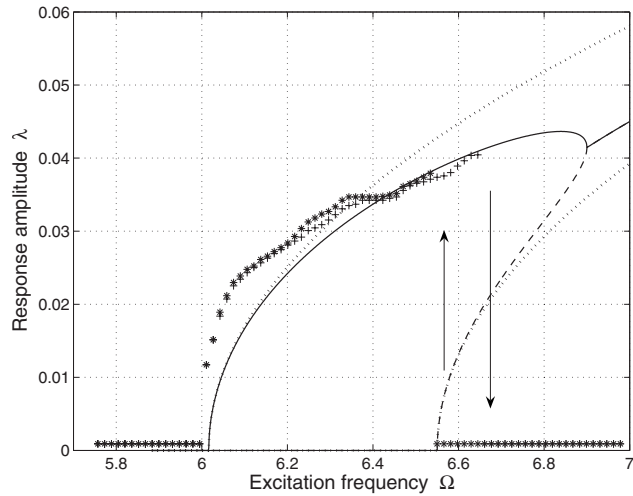


**Fig. 8** Frequency responses. Measured (+: sweep up, \*: sweep down), predicted with damping (---: unstable branch, -: stable branch), and predicted without damping (..).  $\varepsilon=0.17$ ,  $\hat{\alpha}=495$ ,  $\hat{\chi}=71.7$ .

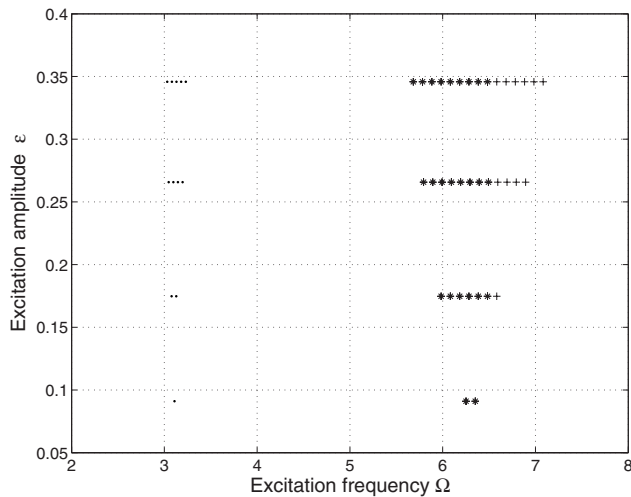


**Fig. 7** Parametric instability region for varying amplitude and frequency; observed instabilities (: secondary instability region, +: sweep up, \*: sweep down)

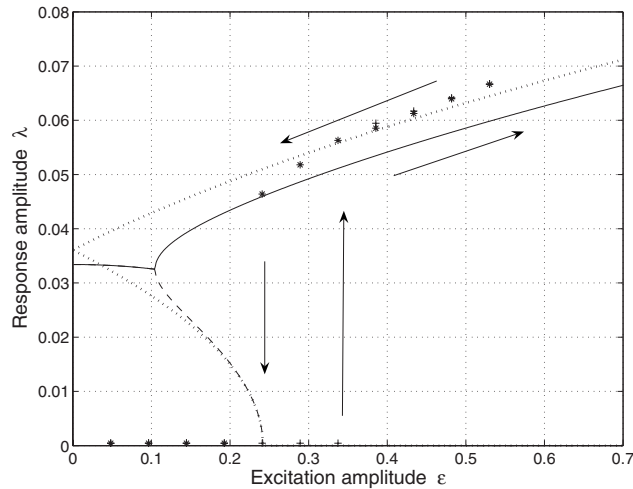


**Fig. 9** Force response. Measured (+: tuning up, \*: tuning down), predicted with damping (---: unstable branch, -: stable branch), and predicted without damping (..).  $\Omega=6.4$ ,  $\hat{\alpha}=495$ ,  $\hat{\chi}=71.7$ .

quency. Nevertheless, this result might be affected by the nonhomogeneous boundary conditions and interaction between transversal, longitudinal, and torsion modes.

## 5 Conclusion

The presented experimental and theoretical investigation shows that automotive multiribbed belts exhibit large transverse vibrations and important nonlinear and parametric instability features. By keeping all the nonlinear terms in the equations, including longitudinal damping and using the multiple scales method, the nonlinear response versus forcing frequency or forcing amplitude shows a hysteretic behavior due to the jumps, which depend on the sweep up and sweep down. Moreover, the experimental setup highlights other nonlinear phenomena: the coupling between longitudinal and torsion behaviors, the coupling between the longitudinal mode shape and the third transverse mode shape, and the presence of a time-varying boundary condition, not considered in the presented theoretical investigation.

## Acknowledgment

The authors wish to thank Valeo electrical system, which has partly supported this work.

## References

- [1] Beikmann, R. S., Perkins, N. C., and Ulsoy, A. G., 1997, "Design and Analysis of Automotive Belt Drive Systems for Steady State Performance," *ASME J. Mech. Des.*, **119**, pp. 162–168.
- [2] Zhang, L., and Zu, J. W., 1999, "One-to-One Auto-Parametric Resonance in Serpentine Belt Drive Systems," *J. Sound Vib.*, **232**, pp. 783–806.
- [3] Bechtel, S. E., Vohra, S., Jacob, K. I., and Carlson, C. D., 2000, "The Stretching and Slipping of Belts and Fibers on Pulleys," *ASME J. Appl. Mech.*, **67**, pp. 197–206.
- [4] Gerbert, G. and Sorge, F., 2002, "Full Sliding Adhesive-Like Contact of V-Belts," *ASME J. Mech. Des.*, **124**, pp. 706–712.
- [5] Kong, L., and Parker, R. G., 2005, "Steady Mechanics of Belt-Pulley Systems," *ASME J. Appl. Mech.*, **72**, pp. 25–34.
- [6] Leamy, M. J., and Perkins, N. C., 1998, "Nonlinear Periodic Response of Engine Accessory Drives With Dry Friction Tensioners," *ASME J. Vib. Acoust.*, **120**, pp. 909–916.
- [7] Michon, G., Manin, L., and Dufour, R., 2005, "Hysteretic Behavior of a Belt Tensioner, Modeling and Experimental Investigation," *J. Vib. Control*, **11**(9), pp. 1147–1158.
- [8] Parker, R. G., and Lin, Y., 2004, "Parametric Instability of Axially Moving Media Subjected to Multifrequency Tension and Speed Fluctuation," *ASME J. Appl. Mech.*, **68**, pp. 49–57.
- [9] Pellicano, F., Cattellani, G., and Fregolent, A., 2004, "Parametric Instability of Belts, Theory and Experiments," *Comput. Struct.*, **82**, pp. 81–91.
- [10] Mockensturm, E., Perkins, N., and Ulsoy, A., 1996, "Stability and Limit Cycles of Parametrically Excited, Axially Moving Strings," *ASME J. Vib. Acoust.*, **118**, pp. 346–351.
- [11] Mockensturm, E., and Guo, J., 2005, "Nonlinear Vibration of Parametrically Excited Viscoelastic Axially Moving Media," *ASME J. Appl. Mech.*, **72**, pp. 374–380.
- [12] Berlioz, A., and Lamarque, C. H., 2005, "A Non-Linear Model for the Dynamic of an Inclined Cable," *J. Sound Vib.*, **279**, pp. 619–639.
- [13] Perkins, N. C., 1992, "Modal Interactions in the Nonlinear Response of Elastic Cables Under Parametric/External Excitation," *Int. J. Non-Linear Mech.*, **27**(2), pp. 233–250.
- [14] Rega, G., and Benedettini, F., 1989, "Planar Non-Linear Oscillations of Elastic Cables Under Subharmonic Resonance Conditions," *J. Sound Vib.*, **132**(3), pp. 367–381.
- [15] Berlioz, A., Der Hagopian, J., Dufour, R., and Draoui, E., 1996, "Dynamic Behavior of a Drill-String. Experimental Investigation of Lateral Instabilities," *ASME J. Vib. Acoust.*, **118**, pp. 292–298.
- [16] Dufour, R., and Berlioz, A., 1998, "Parametric Instability of a Beam Due to Axial Excitations and to Boundary Conditions," *ASME J. Vib. Acoust.*, **120**, pp. 461–467.
- [17] Thurman, A. L., and Mote, Jr., C. D., 1969, "Free, Periodic, Non-Linear Oscillation of an Axially Moving String," *ASME J. Appl. Mech.*, **36**, pp. 83–91.
- [18] Nayfeh, A. H., and Mook, D. T., 1979, *Nonlinear Oscillations*, Wiley, New York.
- [19] Orloske, K., Leamy, M. J., and Parker, R. G., 2006, "Flexural-Torsion Buckling of Misaligned Axially Moving Beam. I. Three-Dimensional Modeling, Equilibria, and Bifurcations," *Int. J. Solids Struct.*, **43**, pp. 4297–4322.
- [20] Orloske, K., and Parker, R. G., 2006, "Flexural-Torsion Buckling of Misaligned Axially Moving Beam. II. Vibration and Stability Analysis," *Int. J. Solids Struct.*, **43**, pp. 4323–4341.